UNIVERSITAT POLITÈCNICA DE CATALUNYA

Laboratory of Photonics
Electromagnetics and Photonics Engineering group
Dept. of Signal Theory and Communications

OPTICAL SOLITONS IN QUADRATIC NONLINEAR MEDIA AND APPLICATIONS TO ALL-OPTICAL SWITCHING AND ROUTING DEVICES

Autor: María Concepción Santos Blanco
Director: Lluís Torner

Barcelona, january 1998

Chapter 5

The Walk-off Parameter: Families of Walking Solitons

So far, the only bright stationary solutions to the system defined by equations (2.94) that have been shown to exist feature a pure linear phase front for both harmonics and in the spatial case are only possible in the absence of walk-off. Walking solitons of this kind are trivial copies of the non-walking ones for any transverse velocity and are excited through input spatial phase modulations introducing some non vanishing momentum into the system (4.15).

Nevertheless, numerical beam propagation methods evidence the possibility to obtain other walking structures in the presence of walk-off which display differentiate characteristics depending on its transverse walking velocity. Therefore this section concentrates on finding numerically the families of walking solitons through the use of the more general ansatz (3.1a) thus accounting for more complicated transverse phase fronts and lifting the restriction of non local energy exchange both between harmonics and between transverse points in the frame of reference moving with the walking velocity.

The solitons found will be shown to exhibit new features as compared with those existing in absence of walk-off. Investigation of these new features is important regarding their potential applications, but also from a fundamental point of view because the approach and outcome have implications to walking solitons existing in other physical settings. Shown here is the one-dimensional case but walking solitons exist also in 2+1 structures [127]-[132].

5.1 The search

5.1.1 Search strategy

The present search as pointing at more general traveling wave structures requires to resort to the generic expression (3.1a)

$$a_{1,2}(s,\xi) = U_{1,2}(s - v\xi)\exp(j\kappa_{1,2}\xi)\exp\left(j\phi_{1,2}(s - v\xi)\right), \tag{5.1a}$$

where v stands for the soliton velocity. As before, it is assumed that the traveling wave solutions to the system are fully stationary and therefore no periodic states are searched for. A necessary requirement for a traveling wave object made up by nonlinear parametric interaction between fundamental and second harmonic waves to be formed is that the linear phase mismatch between the two harmonics results nonlinearly counteracted, the so-called phase-locking condition, i.e. $\kappa_2 = 2\kappa_1 + \beta$. That entails that a traveling wave structure is totally defined by specification of 4 real functions of the transverse coordinate, namely $U_1(\eta)$, $U_2(\eta)$, $\phi_1(\eta)$, $\phi_2(\eta)$ together with 6 free parameters, i.e. r, α, β, δ, κ_1 and v. In the spatial case r is exactly set to $r = -1$ which leaves up to 5 parameters to determine the stationary solutions. Three of them, α, β, δ, are linear parameters that characterize the optical setting whereas κ_1 and v, have a nonlinear nature and parametrize the families of walking solitons. Recall that for interpretation of the results in terms of experimentally relevant quantities one is restricted to small values of v.

The search focuses on bright amplitude profiles. As for the phase profiles one could naïvely expect in analogy with solitons found in the $\delta = 0$ case, that they will need to ensure absence of interharmonics local energy exchange and hence verify $\phi_2 = 2\phi_1$ even though the transverse dependence will be more complicated than the simple linear tilt, but that assumption yielded no hits in the numerical search. Instead, a more generic assumption namely ϕ_2 and ϕ_1 independent but antisymmetric functions ensuring that all local energy exchanges at one side of the $\eta = 0$ points are refunded at the other side so that the total energy into each harmonic is maintained, i.e.

$$\frac{dI_2}{d\xi} = -2\int U_1^2 U_2 \sin\left((2\kappa_1 - \kappa_2 + \beta)\xi + 2\phi_1 - \phi_2\right) ds = 0, \tag{5.2}$$

did allow through a Newton-Raphson numerical scheme to obtain the walking solitons families whose main characteristics are summarized in section 5.3. The local energy losses and excesses produced by the antisymmetric interharmonics energy exchanges are relieved through the action of internal energy dragging inside each harmonic.

Thus the requirement for maintenance of the traveling amplitude profiles is generalized to proper equilibrium between local energy exchanges within harmonics and within other transverse points rather than total absence of all kind of local energy exchanges as for the solutions with $\delta = 0$, i.e. as obtained in (2.115), (2.116)

$$2U_1^2 U_2 \sin(\triangle\psi) = \left(\left(r\psi_{1_s} + v\right) U_1^2\right)_s, \tag{5.3}$$

$$2U_1^2 U_2 \sin(\triangle\psi) = \left(\left(\alpha\psi_{2_s} + (\delta + v)\right) U_2^2\right)_s, \tag{5.4}$$

which in terms of the functions in the ansatz (5.1a) and assuming fulfillment of the phase-locking condition may be written

$$2U_1^2 U_2 \sin(\triangle\phi) = -\left(\left(r\phi_{1_s} + v\right) U_1^2\right)_s, \tag{5.5}$$

$$2U_1^2 U_2 \sin(\triangle\phi) = \left(\left(\alpha\phi_{2_s} + (\delta + v)\right) U_2^2\right)_s, \tag{5.6}$$

stating that into each transverse point the ratios at which the energy leaves or else arrives from the other harmonic must equal that arriving or leaving for other transverse points with the net result that into each individual transverse point no local amplitude changes are observed. Since the total energy in the system is maintained, that entails that the energy a given harmonic receives from the other, as dragged towards other transverse points must entirely be returned at a different transverse position. Maintenance of the harmonics amplitude profiles can thus be viewed as an energy circulating loop which follows the sequence

$$\begin{array}{ccc} FF(s = s_1) & \Longrightarrow & FF(s = s_2) \\ \Uparrow & & \Downarrow \\ SH(s = s_1) & \Longleftarrow & SH(s = s_2) \end{array}$$

whereupon it is expected that both energy exchange and energy dragging are uneven functions

of the transverse variable which since the interest is in bright amplitude profiles entails uneven phase profiles, a datum to bear in mind in the numerical search.

The system of four equations required for the four functions of the traveling wave variable to be determined is completed by adding to (5.5-5.6) the equations for the phases evolution in (2.119), (2.120) which recalling that for equivalence with the ansatz (5.1a) one has $\psi_\xi = \kappa - v\phi_s$, yield

$$\frac{r}{2}U_{1_{ss}} + \left(\kappa_1 - v\phi_{1_s} - \frac{r}{2}\left(\phi_{1_s}\right)^2\right)U_1 - U_1U_2\cos\left(\Delta\phi\right) = 0, \tag{5.7}$$

$$\frac{\alpha}{2}U_{2_{ss}} + \left(\kappa_2 - \left(v+\delta\right)\phi_{2_s} - \frac{\alpha}{2}\left(\phi_{2_s}\right)^2\right)U_2 - U_1^2\cos\left(\Delta\phi\right) = 0. \tag{5.8}$$

Now the system of four equations that will lead to unveiling the transverse profiles of the walking solitons is pertinently written

$$\phi_{1_{ss}} = -2\left(\phi_{1_s} + \frac{v}{r}\right)\frac{U_{1_s}}{U_1} - \frac{2}{r}U_2\sin\left(2\phi_1 - \phi_2\right), \tag{5.9}$$

$$\phi_{2_{ss}} = -2\left(\phi_{2_s} + \frac{\left(v+\delta\right)}{\alpha}\right)\frac{U_{2_s}}{U_2} + \frac{2}{\alpha}\frac{U_1^2}{U_2}\sin\left(2\phi_1 - \phi_2\right), \tag{5.10}$$

$$U_{1_{ss}} = \frac{2}{r}\left(\left(-\kappa_1 + v\phi_{1_s} + \frac{r}{2}\left(\phi_{1_s}\right)^2\right)U_1 + U_1U_2\cos\left(2\phi_1 - \phi_2\right)\right), \tag{5.11}$$

$$U_{2_{ss}} = \frac{2}{\alpha}\left(\left(-2\kappa_1 - \beta + \left(v+\delta\right)\phi_{2_s} + \frac{\alpha}{2}\left(\phi_{2_s}\right)^2\right)U_2 + U_1^2\cos\left(2\phi_1 - \phi_2\right)\right). \tag{5.12}$$

The search focuses on bright amplitude profiles entailing as discussed uneven phase profiles whereupon the initial conditions provided to the numerical integration algorithm read

$$\begin{aligned}
U_1\left(0\right) &= A_1,\\
U_2\left(0\right) &= A_2,\\
\phi_1\left(0\right) &= 0,\\
\phi_2\left(0\right) &= 0,\\
U_{1_s}\left(0\right) &= 0,\\
U_{2_s}\left(0\right) &= 0,\\
\phi_{1_s}\left(0\right) &= A_3,\\
\phi_{2_s}\left(0\right) &= A_4.
\end{aligned} \tag{5.13}$$

A connection may be established between the four constants through use of the first integral of the governing equations which is nothing but the requirement of equilibrium between energy exchanges

$$\left(r\phi_{1_s}(0)+v\right)U_1^2(0)+\left(\alpha\phi_{2_s}(0)+v+\delta\right)U_2^2(0)=0, \tag{5.14}$$

leading to search in a three parameters space with no clues on the approximate values region where to search. Application of the simple shooting method to this problem appears as a crazy task and therefore the option was taken to first search for a more convenient search method which is explained in next section.

5.1.2 The Newton-Raphson root finding method

This section summarizes the basic guidelines to follow for correct implementation of a Newton Raphson method for numerically finding solutions to nonlinear systems of equations with emphasis on those aspects of special relevance in the specific problem of finding the stationary walking solutions in the presence of walk-off.

As a root finding scheme, the Newton Raphson is primarily intended to solve equations with an *algebraic* expression rather than the *differential* equations that one here intends to solve. Luckily enough, the difference is melted down by the magic of numerics allowing through numerical evaluation of the derivatives for the transformation of the system of 4 differential equations into a system of $4\times N$ algebraic equations, with N being the number of points used to discretize the differentiation variable, the transverse coordinate in this case. One obtains

$$\begin{aligned}
&\left(\phi_1^{(i+1)}+\phi_1^{(i-1)}-2\phi_1^{(i)}\right)U_1^{(i)}+2\left(\phi_1^{(i+1)}-\phi_1^{(i-1)}\right)\left(U_1^{(i+1)}-U_1^{(i-1)}\right)\\
&+2\tfrac{v}{r}\left(U_1^{(i+1)}-U_1^{(i-1)}\right)ds+\tfrac{2}{r}U_1^{(i)}U_2^{(i)}\sin\left(\Delta\phi^{(i)}\right)ds^2=0,\\
&\left(\phi_2^{(i+1)}+\phi_2^{(i-1)}-2\phi_2^{(i)}\right)U_2^{(i)}+2\left(\phi_2^{(i+1)}-\phi_2^{(i-1)}\right)\left(U_2^{(i+1)}-U_2^{(i-1)}\right)\\
&+2\tfrac{(v+\delta)}{\alpha}\left(U_2^{(i+1)}-U_2^{(i-1)}\right)ds-\tfrac{2}{\alpha}\left(U_1^{(i)}\right)^2\sin\left(\Delta\phi^{(i)}\right)ds^2=0,\\
&-\left(U_1^{(i+1)}+U_1^{(i-1)}-2U_1^{(i)}\right)-\tfrac{2}{r}\kappa_1U_1^{(i)}ds^2+v\left(\phi_1^{(i+1)}-\phi_1^{(i-1)}\right)U_1^{(i)}ds\\
&+\tfrac{r}{2}\left(\phi_1^{(i+1)}-\phi_1^{(i-1)}\right)^2U_1^{(i)}+U_1^{(i)}U_2^{(i)}\cos\left(\Delta\phi^{(i)}\right)ds^2=0,
\end{aligned} \tag{5.15}$$

$$-\left(U_2^{(i+1)}+U_2^{(i-1)}-2U_2^{(i)}\right)-\tfrac{2}{\alpha}\kappa_2 U_2^{(i)}ds^2+(v+\delta)\left(\phi_2^{(i+1)}-\phi_2^{(i-1)}\right)ds$$
$$+\tfrac{\alpha}{2}\left(\phi_2^{(i+1)}-\phi_2^{(i-1)}\right)^2 U_2^{(i)}+\left(U_1^{(i)}\right)^2\cos\left(\Delta\phi^{(i)}\right)ds^2=0,$$

where the superindex $1\leq i\leq N$ indicates the transverse point in the discretization where the function is evaluated. The system is conveniently expressed in contracted form as

$$A\overrightarrow{x}=0, \tag{5.16}$$

where A is a $4N\times 4N$ matrix and $\overrightarrow{x}=\left[U_1^{(1)},U_2^{(1)},\phi_1^{(1)},\phi_2^{(1)}...,U_1^{(N)},U_2^{(N)},\phi_1^{(N)},\phi_2^{(N)}\right]$ is the vector of unknown quantities.

Now, given a system of algebraic equations $F_i(\overrightarrow{x})=0$, the Newton-Raphson algorithm tries to build up its exact solution , $\overrightarrow{x}_s$, starting from an approximate guess, $\overrightarrow{x}_g$. This is done by considering the Taylor expansion of the system $F_i(\overrightarrow{x})$ around the point $\overrightarrow{x}_g$ as applied to the point $\overrightarrow{x}_s$.

$$F_i(\overrightarrow{x}_s)=F_i(\overrightarrow{x}_g)+\frac{\partial}{\partial\overrightarrow{x}}F_i(\overrightarrow{x}_g)(\overrightarrow{x}_s-\overrightarrow{x}_g)+\frac{1}{2}\frac{\partial^2}{\partial\overrightarrow{x}^2}F_i(\overrightarrow{x}_g)(\overrightarrow{x}_s-\overrightarrow{x}_g)^2+...=0. \tag{5.17}$$

The initial guess would rather be good since only terms up to first order are retained from this expression so to yield the following simple formula for the calculus of the error, $\overrightarrow{e}=\overrightarrow{x}_s-\overrightarrow{x}_g$,

$$\mathcal{J}\overrightarrow{e}=-F(\overrightarrow{x}_g), \tag{5.18}$$

where $\mathcal{J}$ stands for the Jacobian of the system of equations fulfilling $\mathcal{J}_{ij}=\partial F_i/\partial x_j$. The above equation is readily solved through LU decomposition to give a correction to the value of $\overrightarrow{x}_g$ which hopefully is slightly closer to the actual solution. The new guess comes through

$$\overrightarrow{x}_{g_{NEW}}=\overrightarrow{x}_{g_{OLD}}+\overrightarrow{e}. \tag{5.19}$$

Nothing prevents from applying again the same procedure using this new guess, starting an iterative procedure only stopped when the required accuracy to the value of $\overrightarrow{x_s}$ is reached.

This numerical approach has allowed to find the stationary walking solitons presented in next section.

5.2 The family

This section presents the basic features of the families of stationary solitary waves existing in the presence of walk-off. Opposing the solitary waves existing in the absence of walk-off, when walk-off is present the specific transverse dependences as well as the power sharing between harmonics do depend upon the transverse velocity with which they walk the z axis off in such a way that certain power distributions can only be found traveling at given transverse velocities. Due to this and other special features the solitary waves existing with non-zero walk-off have taken to be referred as *walking solitons.*

Families of walking solitons were found to exist with different values of linear wave and material parameters in the system, α, β and δ and within different ranges of wave intensities and soliton velocities. The families of walking solitons existing in a given physical setting, i.e. with fixed α, β and δ, are defined by two independent parameters, namely the total energy flow, I, or the nonlinear wavenumber, κ_1, and the transverse velocity v. In Figure 5-1 the curves relating I and κ_1 are plotted for different v values and two different signs of the wavevector mismatch. For comparison, the curve for the nonwalking solitons has also been included.

The results displayed correspond to $\alpha = -1/2$ allowing interpretation in terms of solitary beam propagation.

The shape and related properties of the walking solitons depend strongly on the various parameters involved and in particular on their velocity. In Figures 5-2 to 5-9 some examples of walking solitons profiles for $\delta = 1$, $\kappa_1 = 3$ and different transverse velocities in both real and imaginary part form, and amplitude and phase front (ϕ_s) form have been displayed. Figures 5-2 to 5-5 correspond to a negative wavevector mismatch value and Figures 5-6 to 5-7 are for a positive one. For correct interpretation of these plots it is important to recall that for given values of δ and β and a fixed value of κ_1, solitons walking with different velocities also carry a different total energy flow, I, as Figure 5-1 shows. Figures 5-8 and 5-9 compare walking solitons carrying the same amount of total power but walking with different transverse velocities.

To further stress the different features displayed by solitons walking at different transverse velocities, Figure 5-10 presents how the total energy is shared between the two harmonics and Figures 5-11 and 5-12 show the respective widths, defined as the full width at half maximum.

Before these plots, it is worth remarking that fast variations of the quantities displayed occur

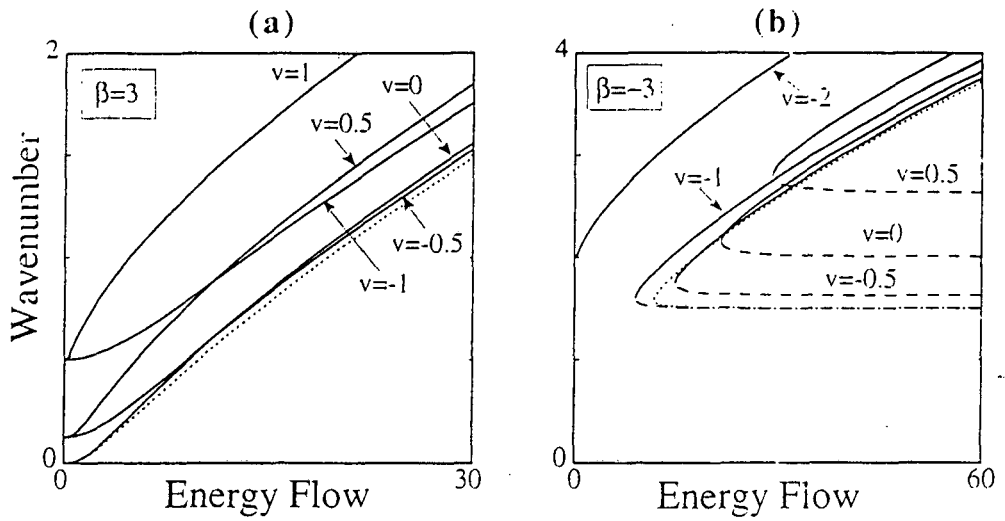

Figure 5-1: Nonlinear wave number shift, κ_1, versus total power for the families of walking soliton solutions for different soliton transverse velocities. In (a): positive wavevector mismatch ($\beta = 3$); in (b): negative wavevector mismatch ($\beta = -3$). In all cases $\delta = 1$. Dashed lines: unstable solutions. Dotted lines: non-walking solitons existing in the absence of Poynting vector walk-off ($\delta = 0$).

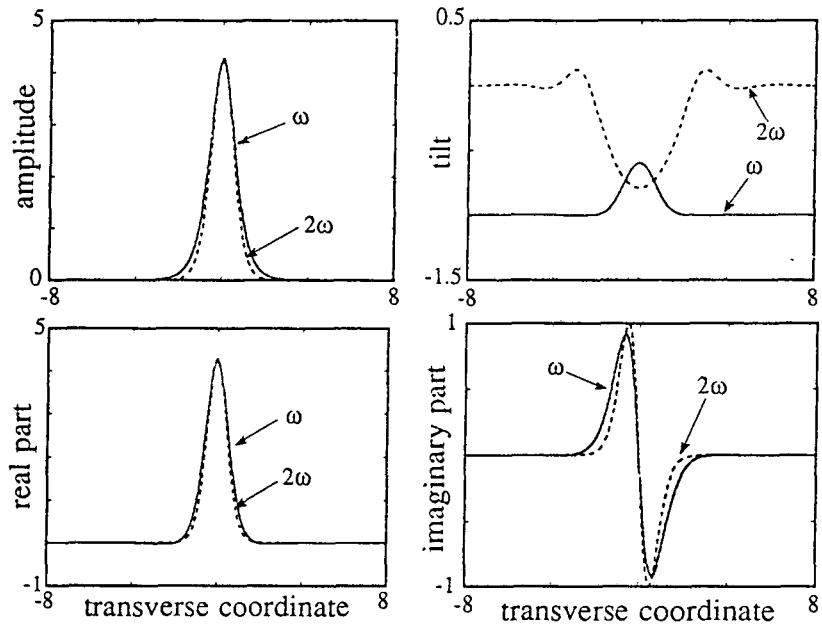

Figure 5-2: Amplitude and phase-front tilt, defined as the transverse derivative of the phase-front; and real and imaginary part profiles for walking solitons with $\beta = -3$, $\delta = 1$, $\kappa_1 = 3$ and $v = -1$.

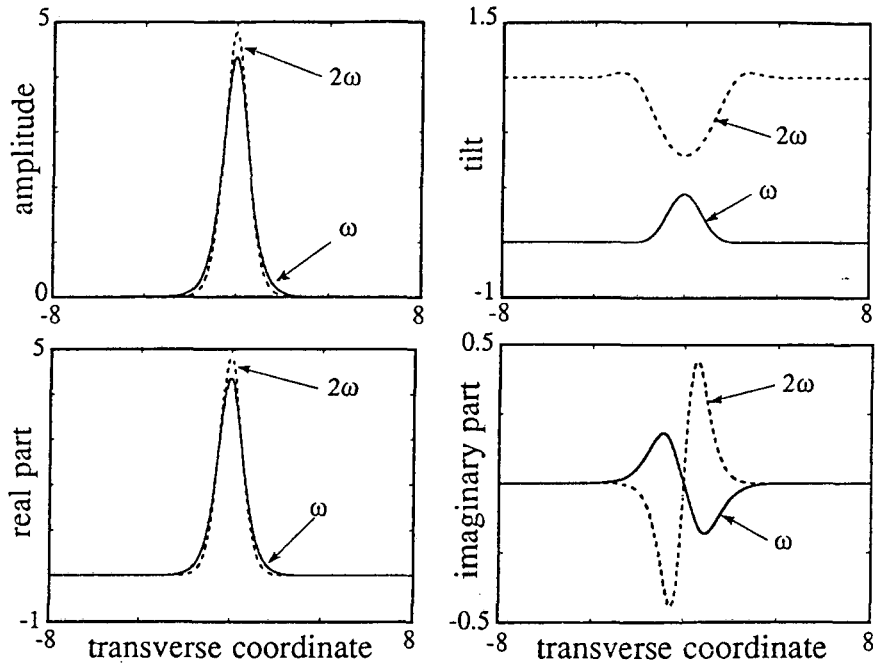

Figure 5-3: Same as Figure 5-2 but with $v = -0.5$.

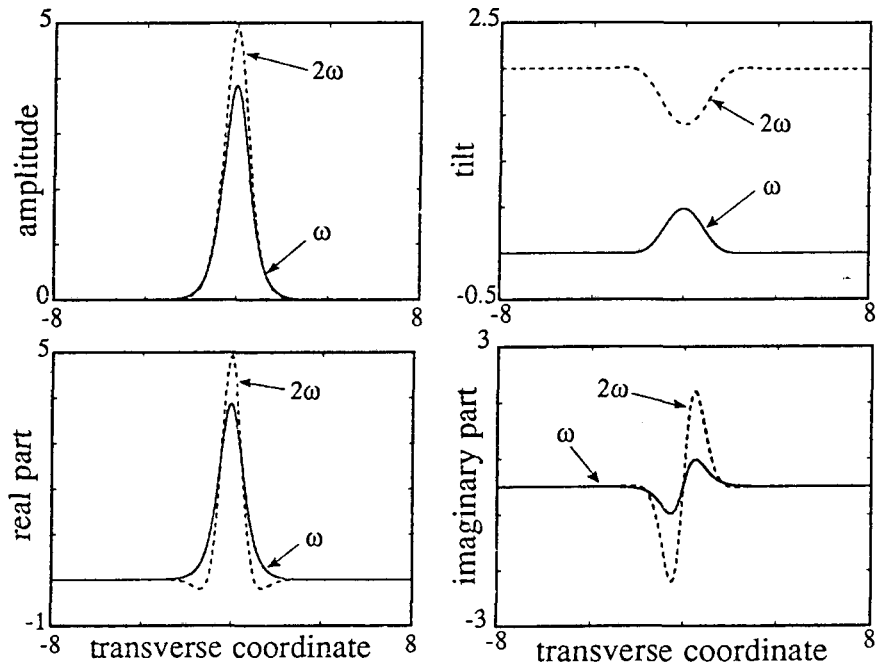

Figure 5-4: Same as Figure 5-2 but $v = 0$.

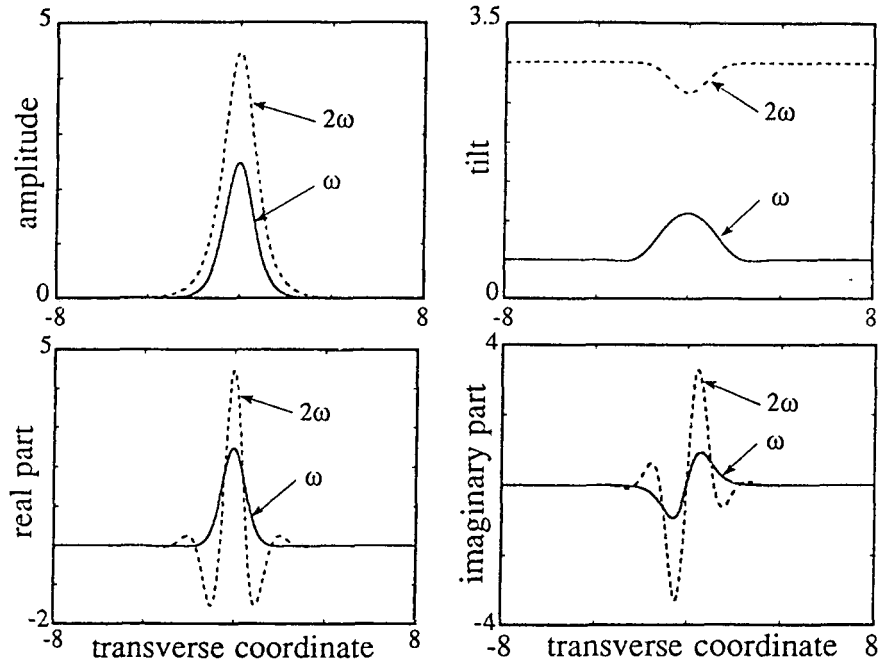

Figure 5-5: Same as Figure 5-2 but $v = 0.5$.

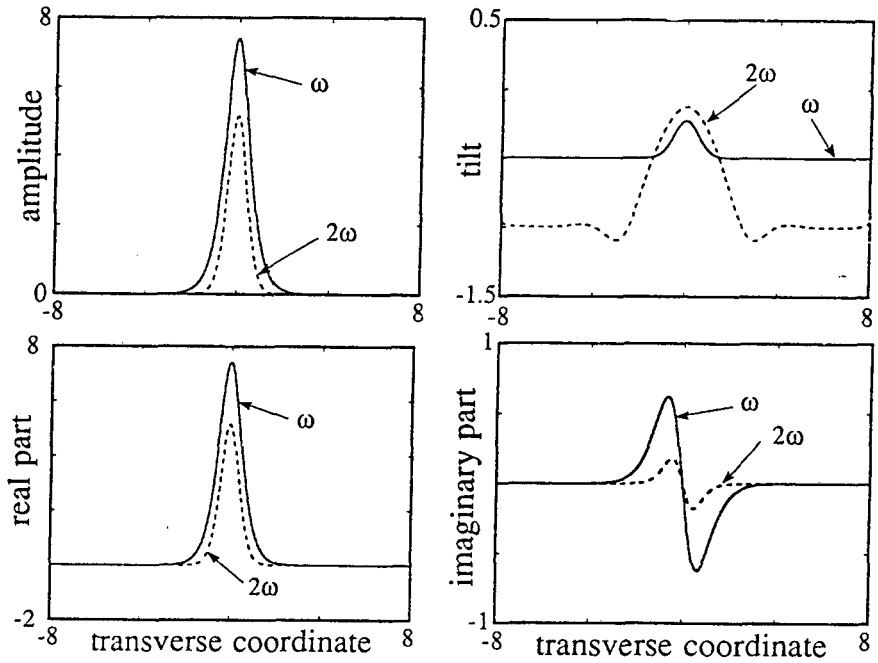

Figure 5-6: Same as Figure 5-2 but for positive wavevector mismatch ($\beta = 3$) and $v = -0.5$.

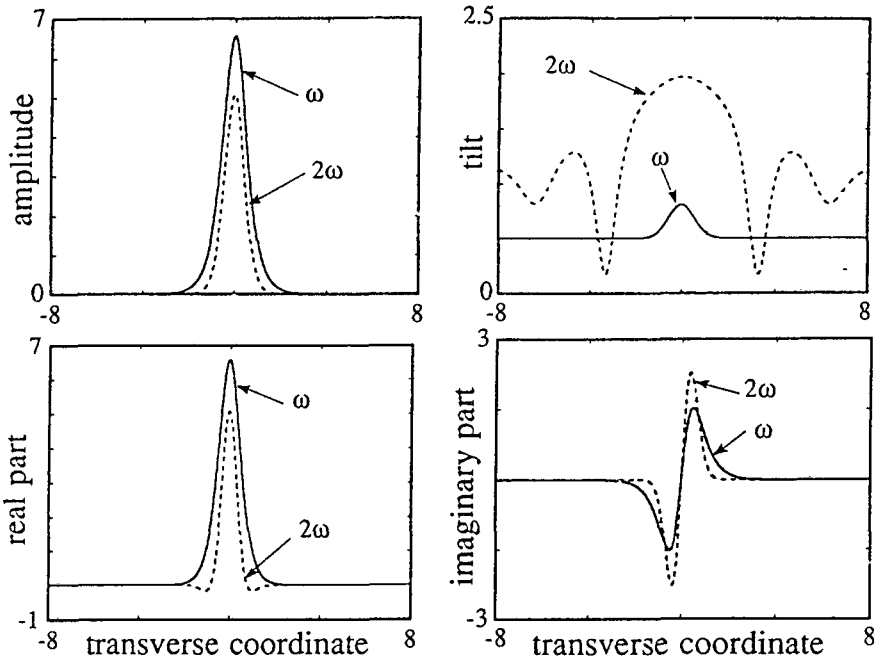

Figure 5-7: Same as Figure 5-6 but for $v = 0.5$.

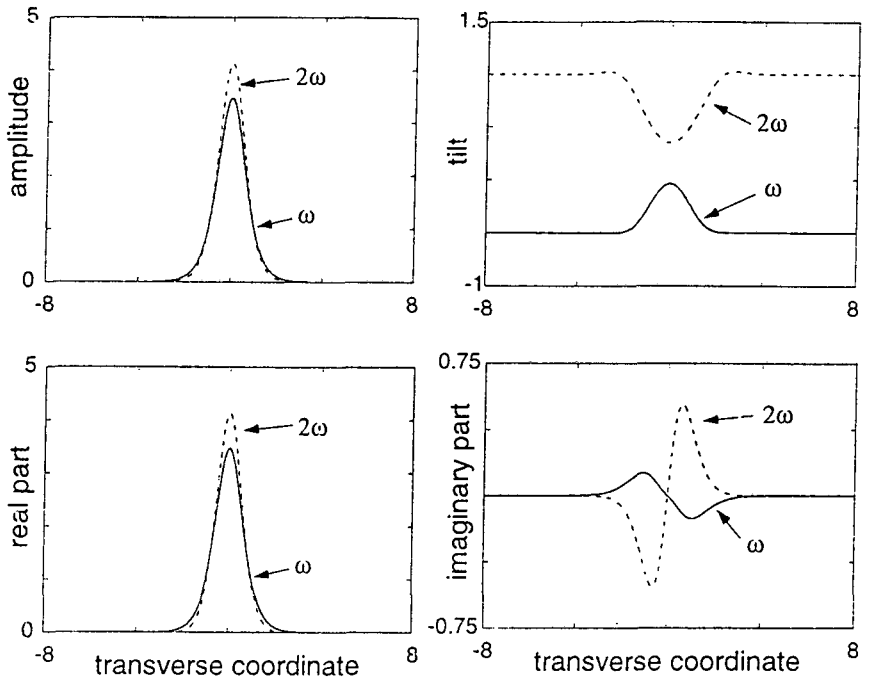

Figure 5-8: Same as Figure 5-3 but for the same energy flow as in Figure 5-9 ($I = 30$). Velocity $v = -0.5$.

when the corresponding soliton families approach their cut-off values, and that in the case of non walking solitons existing when $\delta = 0$ they do not depend upon the transverse velocity of the soliton. The features of the shapes and phase fronts of the walking solitons have crucial implications on their actual experimental excitation. In particular, Fig. 5-1 shows that even in the presence of walk-off, zero-velocity solutions are feasible. However, its excitation requires the input beam to mimic the characteristics of the stationary solution including its precise phase front curvature. Anyway, solitons walking with a pretty small velocity can always be excited with appropriate tilted inputs. This is so provided the Poynting vector walk-off is reasonably small and it is of course at the expense of some loss of energy in the form of radiation.

Similarly, Fig 5-1 b) shows that at negative wavevector mismatch walking solitons exist at energy flows smaller than the minimum threshold energy required for the existence of non walking solitons in the absence of walk-off. This is also a consequence of the phase front curvatures of the walking solitons easing the achievement of the phase locking condition. The actual excitation of low energy solitons with non spatially chirped beams produces a significant amount of radiation, and wide solitons.

The dependence of the threshold energy for the existence of solitons walking with the specific velocities $v = -\delta/2$ and $v = -\delta/4$ is plotted in Figure 5-13 as a function of the walk-off parameter δ, for two values of the wavevector mismatch β. At exact phase matching, for some values of the transverse velocity the existence of walking solitons is restricted to total energy values which exceed a certain energy threshold. Consistent with the scaling rules (3.22) this energy threshold scales as δ^3 and on the other side no energy threshold is found for walking solitons with transverse velocity $v = -\delta/2$.

5.3 Stability

There are different approaches to elucidate the stability of the families of walking solitons. In particular, Etrich and co-workers [130] reported a mathematical proof of the stability criterion obtained through linear stability analysis and studied its application to the case of temporal solitons. Here, a different, geometrical method is used to derive the stability criterion and its implications for the families of spatial walking solitons will be showed in detail.

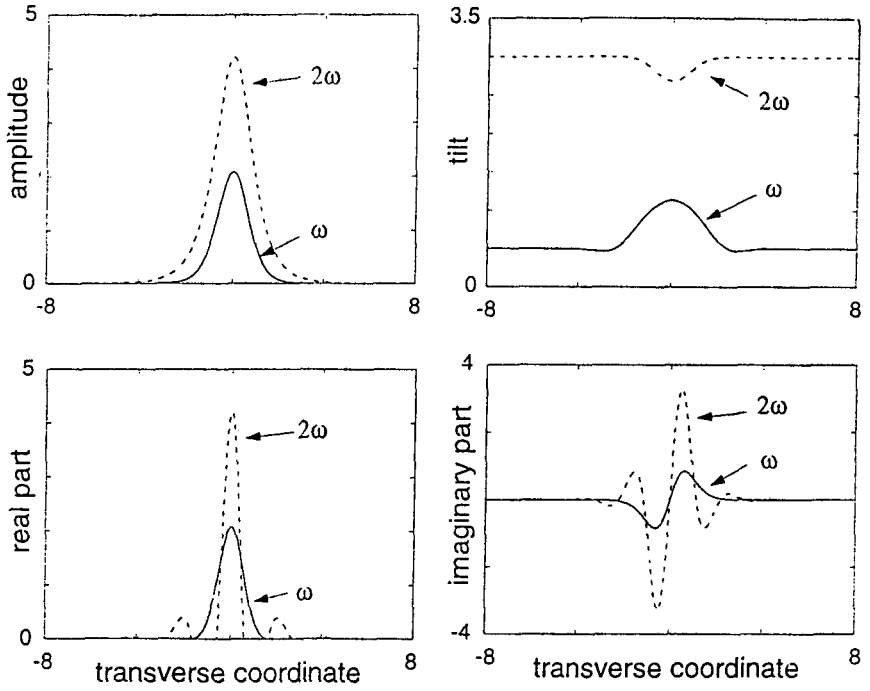

Figure 5-9: Same as Figure 5-5 but for the same energy flow as in Figure 5-8 ($I = 30$). Velocity $v = 0.5$.

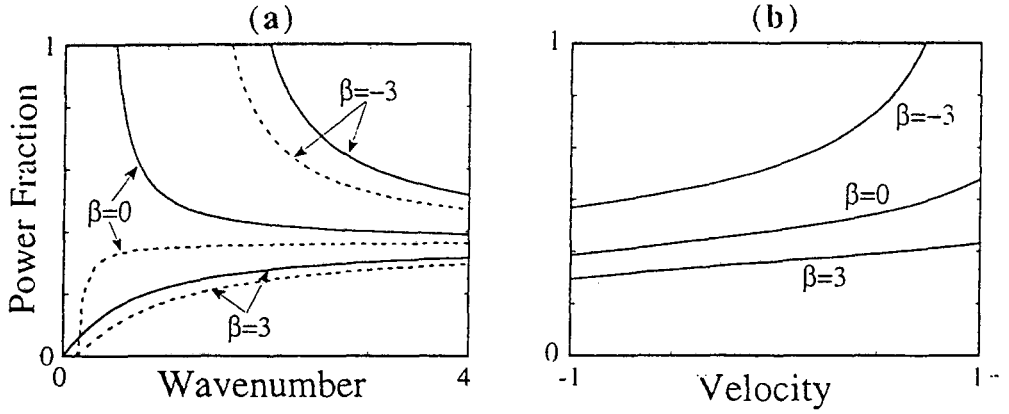

Figure 5-10: Fraction of power carried by the second-harmonic beam (i.e. I_2/I) for representative walking solitons existing at different wavevector mismatches, as a function of the two parameters that define the family of solutions. In (a) the velocity is fixed ($v = -0.5$); in (b) the nonlinear wavenumber shift is fixed ($\kappa_1 = 3$). In all cases $\delta = 1$.

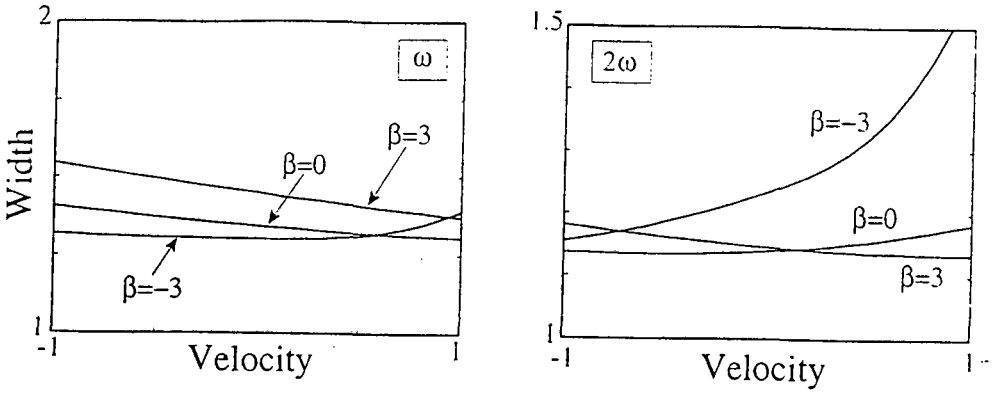

Figure 5-11: Width (FWHM) of the fundamental and second-harmonic beams of representative walking solitons existing at different wavevector mismatches, as a function of the soliton velocity. Here $\kappa_1 = 3$, $\delta = 1$.

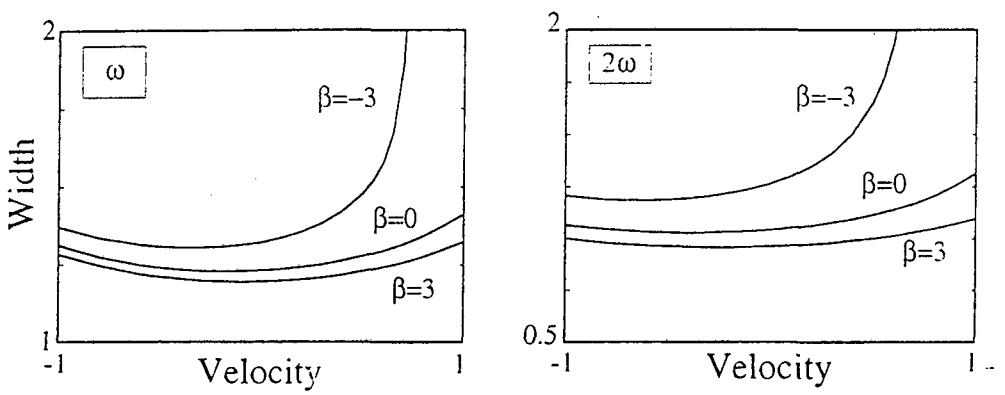

Figure 5-12: Same as Figure 5.11 but for $I = 40$.

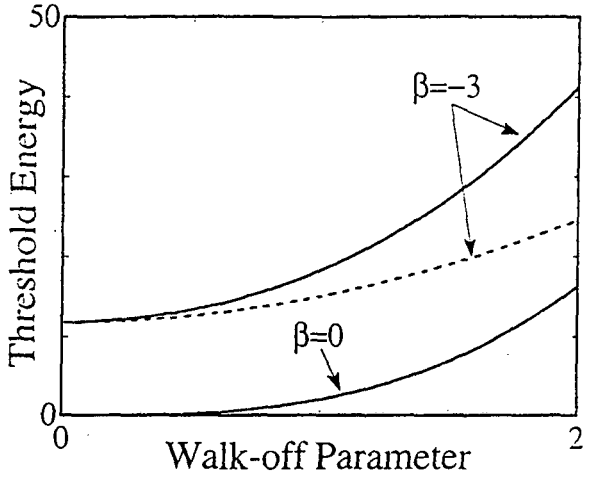

Figure 5-13: Threshold (minimum) energy flow for the existence of solitons walking with a given velocity, as a function of the walk-off parameter δ, for different values of the wavevector mismatch. Continuos lines: threshold energy for solitons walking with a velocity $v = -\delta/2$. At $\beta = 3$ there is no threshold energy for the existence of solitons in the range of walk-off parameters and soliton velocities displayed in the plot.

Again, it is recalled that the analysis is concerned with stability in the same number of transverse dimensions as the system in which the solutions have been found.

The starting point is the variational expression

$$\delta_F \left(H + \kappa_1 I - v J \right) = 0. \tag{5.20}$$

Because the families of stationary walking solitons correspond to the extrema of $\mathcal{H}$ for a given I and $\mathcal{J}$, one can conclude using Lyapunov's theorem that solutions that realize the global minimum of $\mathcal{H}$ are stable whereas those that realize a local extremum may lead to instabilities. According to that, stability elucidation consists in the simple procedure of inspecting the surface $\mathcal{H} = \mathcal{H}(I, \mathcal{J})$ defined by the families of walking solitons and identifying its upper and lower sheets as sketched in Figure 5-14.

Thus the curve of marginal stability separating stable from unstable solutions is in the sketch of Figure 5-14 the curve that separates lower and upper sheets of the $\mathcal{H} = \mathcal{H}(I, \mathcal{J})$ surfaces. One elementary way to determine that curve is by noticing that over the curve the vector normal to the surface is contained on the horizontal plane. Following the sketch in Figure 5-14 express the vector normal to the two-parametric surface $\overrightarrow{r} = I(\kappa_1, v)\,\widehat{x} + \mathcal{J}(\kappa_1, v)\,\widehat{y} + \mathcal{H}(\kappa_1, v)\,\widehat{z}$ as

$$\overrightarrow{n} = \frac{\partial(\mathcal{J}, \mathcal{H})}{\partial(\kappa_1, v)}\widehat{x} + \frac{\partial(\mathcal{H}, I)}{\partial(\kappa_1, v)}\widehat{y} + \frac{\partial(I, \mathcal{J})}{\partial(\kappa_1, v)}\widehat{z}, \tag{5.21}$$

where the symbol $\partial(F, G)/\partial(a, b)$ is used to denote Jacobian matrix of functions F, G with respect to the variables a, b. For this vector to be contained in the horizontal plane the last term in the above expression must vanish, namely

$$\frac{\partial I}{\partial \kappa_1}\frac{\partial \mathcal{J}}{\partial v} - \frac{\partial I}{\partial v}\frac{\partial \mathcal{J}}{\partial v} = 0, \tag{5.22}$$

which thus constitutes the condition of marginal stability for the families of walking solitons. This criterion is more involved than the so-called Vakhitov-Kolokolov criterion, given by

$$\frac{\partial I}{\partial \kappa_1} = 0. \tag{5.23}$$

Subsequently, identification of the stable and unstable walking solitons comes through eval-

uation of the condition (5.22) for the families of walking solitons that exhibit multi-valued surfaces $\mathcal{H} = \mathcal{H}(I, \mathcal{J})$. Otherwise the solutions are always found to correspond to the minima of $\mathcal{H}$ for a given I and $\mathcal{J}$, and hence all members of the family are stable. The whole surfaces $\mathcal{H} = \mathcal{H}(I, \mathcal{J})$ are not easily plotted but there is no need for. For illustrative purposes Figures 5-15 and 5-16 show the projections in the $I - \mathcal{H}$ and $I - \mathcal{J}$ planes corresponding to some of the particular families of walking solitons appearing in Figure 5-1.

The curves in Figure 5-1 already included the outcome of the stability analysis showing in dotted line the unstable solutions. As mentioned above, a extremely small numerical difference is found between the condition of marginal stability given by (5.22) and by (5.23). A typical example is shown in Figure 5-17. Accordingly such a difference has no physical relevance in the cases studied here. This is consistent with the results of the series of numerical simulations conducted for selected members of the families of walking solitons [127] which showed that criterion (5.23) very approximately holds for the families of spatial walking solitons addressed here. The situation may be different in the case of temporal solitons [129], because of the additional degrees of freedom offered by the values of the group velocity dispersion of pulses at the fundamental and second harmonic frequencies.

The main conclusion to be raised is that most of the members of the families of walking solitons are stable on propagation. Some of the solutions that are found near the cut-off condition for the soliton existence would be unstable, but those have a very limited physical relevance to the experimental formation of solitons mainly because in reality the input beams never match exactly its transverse shape and also because for the same value of total energy one can always find an stable solution. Adding to that the fact that the solutions near cut off feature increasingly broader beams it is reasonable to admit that excitation of stable solutions that exist reasonable far from cut off is what dominates the dynamics of beam evolution.

A broad variety of numerical experiments with both stable and unstable solutions were performed always confirming the above expectations. The unstable solutions either spread or they reshape and excite a stable walking soliton of the lower sheet of the $\mathcal{H} = \mathcal{H}(I, \mathcal{J})$ surface.

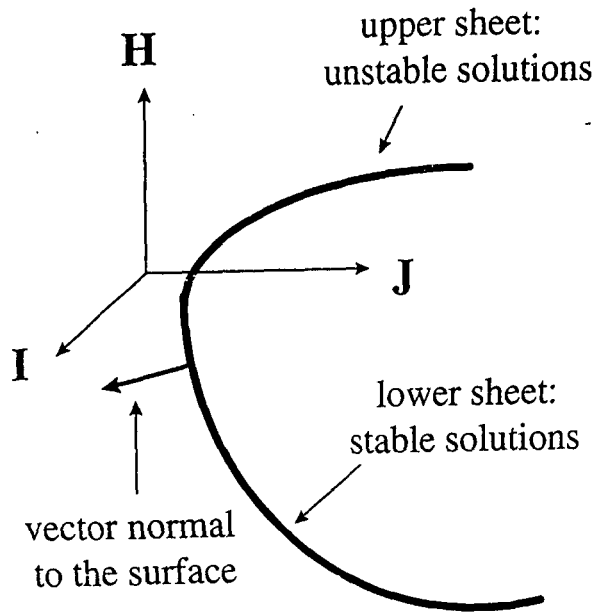

Figure 5-14: Sketch of the procedure to determine geometrically the condition of marginal stability of the walking solitons by examination of the surface energy-momentum-hamiltonian of the families of solutions.

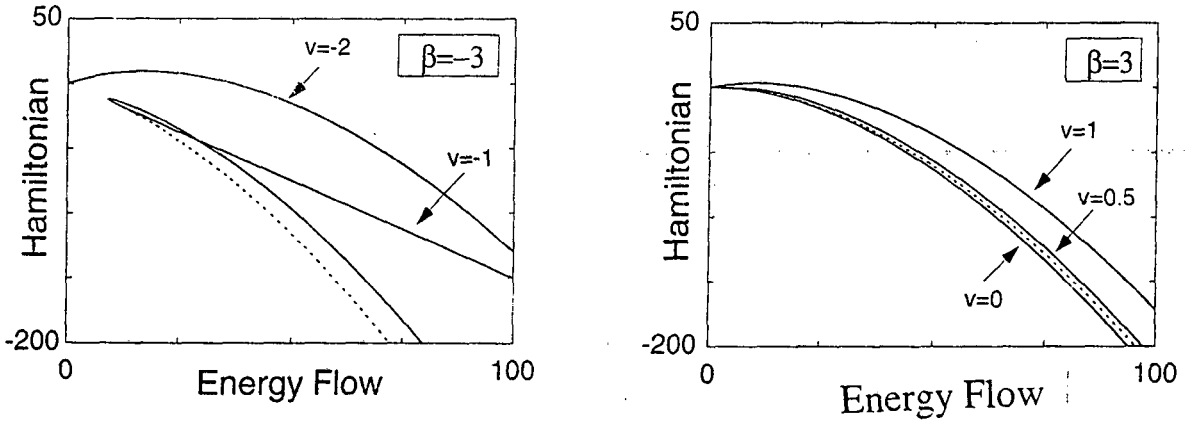

Figure 5-15: Hamiltonian versus energy flow for some of the families of walking solitons of Figure 5-1. Notice that the curves correspond to fixed soliton velocities, but the momentum is not constant along the curves. For the sake of clarity only the curves for a few velocities are shown. Dotted lines: non-walking solitons ($\delta = 0$).

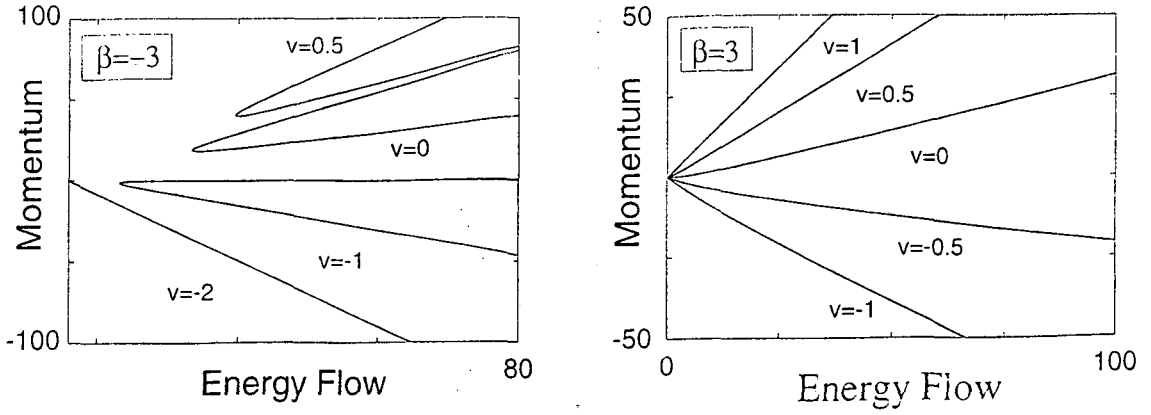

Figure 5-16: Momentum versus energy flow for the families of walking solitons of Fig 5-1. Notice that the hamiltonian is not constant along the curve.

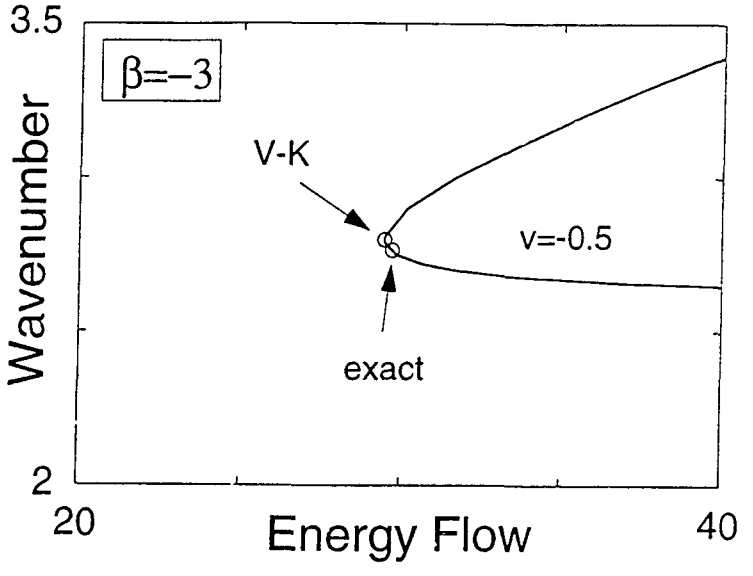

Figure 5-17: Zoom of one representative curve of Figure that shows the very small differences between the numerical values for the condition of marginal stability given by the exact and by the Vakhitov-Kolokolov criterion. Conditions $\beta = -3$, $v = 0.5$.

5.4 Soliton tails

As it was done for the nonwalking solitons, now the problem of elucidating how are the stationary equations fulfilled in tails and which is the transverse dependence there is studied.

As for the amplitude profiles, writing the fields in the form $a_\nu(s,\xi) = U_\nu(\eta)\, e^{j(\kappa_\nu \xi + \phi_\nu(\eta))}$ in the governing equations (2.94), form the real part and neglecting terms coming from nonlinear parametric interaction, exponential decay tails were obtained as

$$U_1 \sim B_1 \exp(-\Gamma_1 s), \tag{5.24}$$

$$U_2 \sim B_2 \exp(-\Gamma_2 s). \tag{5.25}$$

with

$$\Gamma_1^2 = -\frac{2}{r}\kappa_1 - \frac{v^2}{r^2} = 2\kappa_1 - v^2, \tag{5.26}$$

$$\Gamma_2^2 = -\frac{2}{\alpha}\kappa_2 - \frac{(v+\delta)^2}{\alpha^2}, \tag{5.27}$$

where it has been used the fact that in the spatial case r is exactly set to $r = -1$.

The condition for real values for Γ_1 and Γ_2, determines the cut-off value for walking solitons, yielding

$$\kappa_{1_{CUT-OFF}} = \max\left\{\frac{v^2}{2}, -\frac{\beta}{2} - \frac{(v+\delta)^2}{4\alpha}\right\}. \tag{5.28}$$

The assumption behind neglection of nonlinear parametric interaction terms is actually assuming

$$U_2 << 1, \tag{5.29}$$

$$\frac{U_1^2}{U_2} << 1. \tag{5.30}$$

The above assumption (5.30) is only consistent with the results in (5.26-5.27) if $\Gamma_2 < 2\Gamma_1$, that is, when it is verified

$$\frac{1}{\alpha}\left[(2\alpha+1)\left(2\kappa_1 - v^2\right) + v^2 + \beta + \frac{(v+\delta)^2}{2\alpha}\right] > 0, \tag{5.31}$$

which setting $\alpha = -0.5$ leads to

$$v < \frac{\beta}{2\delta} - \frac{\delta}{2}. \tag{5.32}$$

Otherwise, the contribution of nonlinear interaction terms affects the fields dependence in the soliton tails.

Imaginary parts in the governing equations using $a_\nu(s,\xi) = U_\nu(s)\, e^{j(\kappa_\nu \xi + \phi_\nu(s))}$, leads to the equations for the phase profiles, namely

$$-\left(v + r\phi_{1_s}\right) U_{1_s} - \frac{r}{2}\phi_{1_{ss}} U_1 + U_1 U_2 \sin\left(2\phi_1 - \phi_2\right) = 0, \tag{5.33}$$

$$-\left(v + \delta + \alpha\phi_{2_s}\right) U_{2_s} - \frac{\alpha}{2}\phi_{2_{ss}} U_2 + U_1^2 \sin\left(2\phi_1 - \phi_2\right) = 0. \tag{5.34}$$

When nonlinear terms can be neglected, i.e. under the assumption in (5.32), the phase profiles further assuming $\phi_{1_{ss}} \underset{s\to\infty}{\longrightarrow} 0$, $\phi_{2_{ss}} \underset{s\to\infty}{\longrightarrow} 0$ in the soliton tails verify

$$\phi_{1_s} \underset{s\to\infty}{\longrightarrow} -\frac{v}{r}, \tag{5.35}$$

$$\phi_{2_s} \underset{s\to\infty}{\longrightarrow} -\frac{(v+\delta)}{\alpha}. \tag{5.36}$$

When nonlinear parametric interaction terms have a relevant contribution, i.e. when $v > \beta/(2\delta) - \delta/2$, the whole equation in (5.33) must be solved which may yield a ϕ_{2_s} solution with oscillating behavior. Note that ϕ_{2_s} appears as well in the equation for the second harmonic amplitude profile, U_2, (3.69), whereupon determination of the second harmonic tails dependence requires a system of two coupled differential equations to be solved. That may alter the cut-off values as acting upon the second term in brackets in (5.28) but in all the walking solitons found through the numerics the cut-off was determined by the first term.

This analysis of transverse dependences in tails proves useful to understand the reduction of the energy threshold above which stationary solutions are found in the negative β case. Recalling the intuitive vision of the instability displayed by the solutions near cutoff in the $\delta = 0$ case, developed in section 3.5.4, which blamed on the difference in exponentially transverse increasing velocities as evolving from $s \to \infty$ towards $s = 0$ ($\Gamma_2 << \Gamma_1$) for obtention of too broad transverse profiles which prevented achievement of low total energy values in the

solutions and subsequently led to unbalanced oscillating states, one can understand stable soliton formation below the energy flow threshold for non-walking solitons in the $\delta \neq 0$ case by relief on the transverse decaying exponential constants difference allowing attainment of sharp enough transverse profiles and therefore correspondingly low energy values. This intuitive vision proves consistent with the results obtained through the numerics since to ease the differences between the exponential decay constants in the $\beta < 0$ case (5.26-5.27) it is required,

$$|\beta| + (v+\delta)^2 \geq v^2 \longrightarrow v \geq -\frac{\delta}{2} - \frac{|\beta|}{2\delta}. \tag{5.37}$$

In terms of stability one should want the velocity to exceed that threshold, but mind that if v is too big then Γ_1 may be too low so that again one is left with a too big difference between exponentially decaying constants only with a different sign ($\Gamma_1 << \Gamma_2$). That leads to an upper bound for the transverse velocity that allows for energy threshold reduction, namely

$$|\beta| + (v+\delta)^2 \leq v^2 + |\beta| \longrightarrow v \leq -\frac{\delta}{2}. \tag{5.38}$$

Note that the lower bound for v corresponds to the case when $\Gamma_2 = 2\Gamma_1$ which is precisely the condition fulfilled in tails by positive β non-walking solitons and then as it happens for this kind of solitons, there is no energy threshold at all for $v = -\delta/2 - |\beta| / (2\delta)$ as Figure 5-1 shows.

5.5 Excitation of walking solitons

Now that the families of spatial walking solitons and its basic features have been presented and that the majority of experimentally relevant solitons have been shown to be stable on propagation, its excitation from practical conditions appears as a not very easy task because of the complicated phase fronts needed.

Considering the expression, derived from (4.14)

$$v = \frac{\mathcal{J}}{I} - \delta\frac{I_2}{I} - (2\alpha+1)\frac{\mathcal{J}_2}{I}, \tag{5.39}$$

even though for input beams that closely resemble the stationary solutions little effect of radiation is expected and therefore the soliton eventually formed will approximately carry the same

conserved quantities as the input, neither I_2 nor $\mathcal{J}_2$ are conserved quantities and therefore they change dynamically during propagation. In particular, the dynamical evolution of I_2 depends significantly on the material parameters, including the value of δ, and excitation conditions.

First term in (5.39) accounts for transverse tilts or more complicated transverse phase modulations of the beams while the second term stands for the mutual dragging of ordinary fundamental and extraordinary second harmonic beams due to the presence of walk-off being the last term very small in the spatial case.

According to (5.39) the transverse velocity of solitons excited with zero-momentum inputs is approximately $v \sim -\delta I_2/I$. Thus, to estimate the soliton velocity one may consider the I_2/I ratio corresponding to the family of walking solitons. This ratio happens to depend strongly on the linear wavevector mismatch and on the total energy flow. In a wide range of experimentally relevant light intensities at positive β the solitons have small I_2/I, hence they walk slowly. Conversely at phase matching and negative β the solitons I_2/I ratio is larger and therefore the solitons are faster. According to the variation experienced by the ratio I_2/I, when the β absolute value is increased negative β solitons walk still faster and positive β solitons have still lower velocity. Very high energy flows reduce the effective wavevector mismatch given by β in the linear case, thus the ratio I_2/I and the soliton velocity v behave accordingly so that for example at large positive β higher energy solitons walk faster than lower energy solitons. This analysis will be useful in next chapter when the implications of walking solitons to the design of practical devices are investigated.

A detailed discussion of walking solitons formation under a variety of excitation conditions is found in [127]-[132]. Shown here are a few selected cases chosen to stress the physical relevance of all families of walking solitons provided judicious values of δ and v are considered so that both the paraxial and scalar approximations used to derive equations (2.94) hold.

Excitation of a soliton with large velocity was achieved through the use of input tilted beams of the form

$$a_1(\xi = 0, s) = A Sech^2(s) \exp(j\mu s), \tag{5.40}$$

$$a_2(\xi = 0, s) = B Sech^2(s) \exp(j2\mu s). \tag{5.41}$$

Figure 5-18 shows the results. The salient point is that whereas the slow walking soliton

excited with $\mu = 0$ features a higher second harmonic peak, as solitons existing in the absence of Poynting vector walk-off for this β value, for the fast walking soliton which has transverse velocity $v \approx -1.9$ in Figure 5-18 b) it is the fundamental which carries the largest energy. This result is consistent with the properties of the families of walking solitons as a function of the velocity illustrated in Figures 5-2 to 5-5, 5-8 to 5-9 and 5-11 to 5-12. Physically this is so because the phase front curvatures of the walking solitons modify the effective wavevector mismatch across the beam from the nominal value given by β. In terms of the behavior in the soliton tails, as seen in previous section, this threshold reduction is understood from the viewpoint that the harmonics relative leading exponential decay constants approach the condition $\Gamma_2 \simeq 2\Gamma_1$ typical of the $\beta > 0$ non-walkiong solitons in which no threshold at all is displayed.

Some curves in Figure 5-1 correspond to solitons that walk against the Poynting vector walk-off: Figure 5-19 (a) shows one of such solitons that has been excited with $A = B = 4$, and forced to walk against the direction pointed by δ by setting $\mu = 1$. Finally, Fig 5-19 (b) shows the case of a low-energy soliton walking with velocity $v \approx -1.7$ formed at $\beta = -3$ with $A = B = 1$, and $\mu = 1$. Recall that at $\beta = -3$ non-walking solitons in the absence of Poynting vector walk-off do not exist at such low energies but walking solitons do because for these range of velocities they approach the conditions of the positive β case for nonlinear phase matching in the soliton tails.

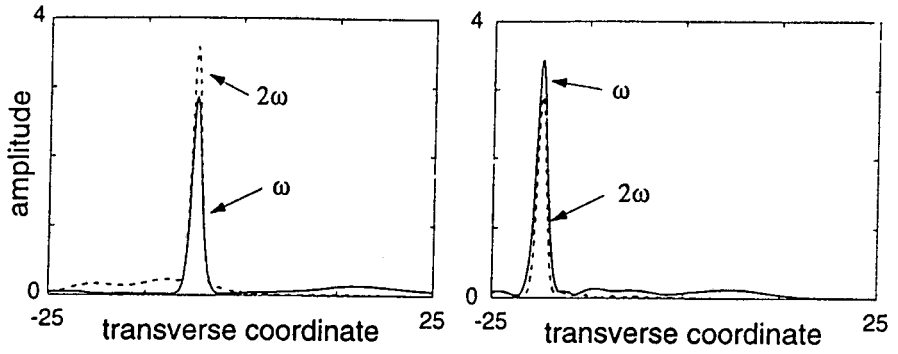

Figure 5-18: Transverse amplitude profiles of the fundamental and second harmonic beams at $\xi = 10$ for selected walking solitons that have been numerically excited with different input tilts and different input conditions. Tilts: (a) $\mu = 0$; (b) $\mu = -1.5$. In both cases $A = 3$, $B = 3$, $\beta = -3$ and $\delta = 1$.

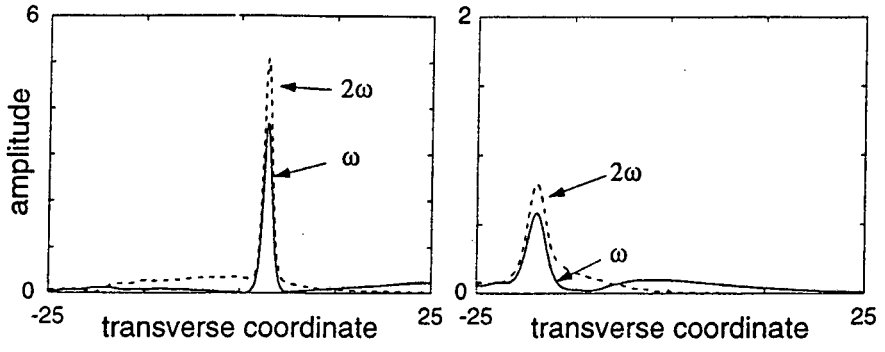

Figure 5-19: Same as in previous Figure, but for other input conditions: (a) $A = 4$, $B = 4$, $\mu = 1$; (b) $A = 1$, $B = 1$, $\mu = -1$. In both cases $\beta = -3$ and $\delta = 1$.